Pergamon

Geochimica et Cosmochimica Acta, Vol. 66, No. 23, pp. 4057–4067, 2002

0016-7037/02 $22.00 + .00

PII S0016-7037(02)00989-4

Spectroscopic and XRD studies of the air degradation of acid-reacted pyrrhotites

YU. L. MIKHLIN,[1,*] A. V. KUKLINSKIY,[1] N. I. PAVLENKO,[1] V. A. VARNEK,[2] I. P. ASANOV,[2] A. V. OKOTRUB,[2] G. E. SELYUTIN,[1] and L. A. SOLOVYEV[1]

[1]Institute of Chemistry and Chemical Technology of the Russian Academy of Sciences, K. Marx Street, 42, Krasnoyarsk 660049, Russia
[2]Institute of Inorganic Chemistry of the Russian Academy of Sciences, pr. Lavrent'eva, 3, Novosibirsk 630090, Russia

(*Received April* 9, 2001; *accepted in revised form June* 7, 2002)

Abstract—Monoclinic and hexagonal pyrrhotites leached in 1 mol/L HCl and exposed to the air at 100% and ~10% relative humidity for up to 5 months were studied using X-ray diffraction, Fourier transform infrared (FTIR) spectroscopy, X-ray photoelectron spectroscopy (XPS), X-ray emission spectroscopy, Mössbauer spectroscopy, and electron paramagnetic resonance (EPR). The amorphous, nonequilibrium, iron-depleted layer (NL) produced by the leaching amounted to half of the residue mass and was composed of predominantly low-spin ferrous iron and polysulfide anions. Elemental sulfur and goethite were the only crystalline products of the NL decomposition. FTIR spectroscopy and XPS also revealed several sulfoxy species and, at low humidity, a small amount of ferric oxide. Neither alterations of the underlying pyrrhotite nor new iron sulfide phases (pyrite, pyrrhotite, etc.) crystallized from the amorphous NL were found. The NL decomposition was faster in the wet environment than in the dry one, and the oxidation of the NL was much more rapid than that of starting pyrrhotites. The intensity and quadruple split of the Mössbauer signal from the product (an isomer shift of 0.36 mm/s) were found to increase over the aging, indicating that the NL structure becomes more rigid and the singlet Fe(II) gradually converts to Fe(III). X-ray Fe Lα,β emission spectra showed the formation of intermediate, high-spin Fe(II) within the NL oxidized in the humid environment, but not in the dry air. No unpaired electron spins were detected by EPR; lines of paramagnetic Fe^{3+} appeared after the samples were aged in the dry air for 49 d and even later in the humid atmosphere. These phenomena are explained in terms of the formation of defects with negative correlation energy, similar to noncrystalline semiconductor chalcogenides, and of the fast electron exchange between the iron species, respectively. Mechanisms for reactions involved with the weathering of iron sulfides, which take into consideration the NL lattice elasticity, S-S and S-O bonding, oxygen incorporation, and oxidative and spin state of iron, are discussed. It is suggested in particular that the surface layer, strongly enriched in sulfur, as well as elemental sulfur and ferric oxyhydroxides, do not inhibit sulfide oxidation and acid production under weathering conditions, but the partially oxidized, disordered, nonstoichiometric layer may be passive.

1. INTRODUCTION

Pyrrhotite, $Fe_{1-x}S$, $0 < x < 0.125$, represents a variety of minerals based on the NiAs structure that contain high-spin Fe^{2+} ions, monosulfide anions, and a system of ordered cation vacancies. Pyrrhotite is one of the most reactive of the sulfide minerals, and its oxidation products contribute significantly to the acidity of solutions seeping from mine waste dumps and tailings of concentrating plants (Steager and Desjardins, 1978; Thornber and Wildman, 1979; Steager, 1982; Nicholson and Scharer, 1994; Murad et al., 1994; Janzen et al., 2000). The process could be described by an arbitrary reaction:

$$Fe_{1-x}S + (2-2m)O_2 + (3-3x)H_2O = (1-x)Fe(OH)_3 + mS^0 + (1-m)SO_4^{2-} + (3-3x)H^+, \quad (1)$$

where $Fe(OH)_3$ and SO_4^{2-} stand for a series of ferric iron oxyhydroxides and sulfate-bearing species, respectively. The reaction kinetics and mechanisms are still poorly understood, and the products remain insufficiently specified (see, e.g., Nicholson and Scharer, 1994). An important feature of pyrrhotite oxidation and dissolution is the formation of a nonstoichiometric nonequilibrium or metastable layer (NL) as a result of preferential release of iron relative to sulfur (Buckley and Woods, 1985a, 1985b; Timoshenko et al., 1991; Jones et al., 1992; Pratt et al., 1994a, 1994b; Mycroft et al., 1995; Pratt and Nesbitt, 1997; Mikhlin et al., 1995, 1998, 2000, 2001; Kuklinskiy et al., 2001):

$$Fe_{1-x}S + 0.5yO_2 + 2yH^+ = Fe_{1-x-y}S + yFe^{2+} + yH_2O, \quad (2)$$

$$Fe_{1-x}S + 0.75yO_2 + 1.5yH_2O = Fe_{1-x-y}S + yFe(OH)_3. \quad (3)$$

Field observations of oxidized sulfide tailings revealed sulfur-rich alteration rims of pyrrhotite grains as well (Blowes and Jambor, 1990). Buckley and Woods (1985a), Pratt et al. (1994a), and Mycroft et al. (1995) used X-ray photoelectron spectroscopy (XPS) and Auger electron spectroscopy (AES) to study pyrrhotite oxidized in air at ambient temperature. The outermost iron oxyhydroxide layer was found to be ~0.5 nm thick; the underlying sulfur-enriched zone (~3 nm thick), in which the S/Fe ratio approached 2, contained disulfide and polysulfide species. Mycroft et al. (1995) suggested that the sulfur-rich zone consists of marcasite-like FeS_2 and Fe_2S_3 layers. Pyrrhotite leaching in acid solutions proceeding via the

* Author to whom correspondence should be addressed (yumikh@icct.ru).

removal of iron from the pyrrhotite structure leaves the metal-depleted zone (often S/Fe $>$ 2) protracted to a depth of several tens or even thousands of nanometers (Timoshenko et al., 1991; Jones et al., 1992; Pratt et al., 1994b; Pratt and Nesbitt, 1997; Mikhlin et al., 1995, 1998, 2000, 2001; Kuklinskiy et al., 2001). The most bulky metal-deficient layer was established to form in the narrow potential range -0.1 to 0 V (vs. Ag/AgCl) and at positive potentials higher than $\sim$0.7 V; in both these regions, pyrrhotite rapidly dissolves, yielding H_2S and elemental sulfur, respectively (Mikhlin, 2000; Kuklinskiy et al., 2001).

The nonstoichiometric layers are extremely widespread and may take a significant part in geochemical cycles of iron and sulfur, determining the reaction rates and products. An understanding of the structure and chemistry of these "phases" is critically important for assessing their reactivity and the potential for transformation to more stable minerals. However, little research into these problems has been carried out so far. Jones et al. (1992) derived from X-ray diffraction (XRD) data that the metal-deficient layer of monoclinic pyrrhotite leached in anoxic perchloric acid solution restructured to a defective tetragonal phase Fe_2S_3 with linear S-S chains, but mostly the NL was amorphous (Timoshenko et al., 1991; Mikhlin et al., 1995, 2000). XPS, X-ray spectroscopy, and Mössbauer spectroscopy (MS) examinations of the electronic structure of the NL formed under nonoxidative conditions proved that it is composed of predominantly low-spin, "pyritic" ferrous iron, along with some high-spin Fe(II) and Fe(III), polysulfide species, and minor oxygen (Mikhlin et al., 1998, 2000). Pratt et al. (1994b) and Pratt and Nesbitt (1997) observed a sequence of textures that developed at monoclinic pyrrhotite reacted in air-saturated solutions of H_2SO_4 and HCl (pH 3) and then aged in air. Four of the textured surfaces were identified as Fe-oxyhydroxide products, despite a concentration of S $>$20 atom %; AES depth profiles showed that sulfur varied antipathetically with oxygen. An oxygen-free underlayer exposed by spalling of the oxyhydroxides was considerably enriched in sulfur over iron. It was assumed that ferric oxyhydroxide coatings, which are maintained under 100% humidity conditions, retard further oxidation of pyrrhotite. Consequently, periodic wetting, drying, and desiccation of the oxyhydroxide layer in waste rock dumps and tailings situated above the water table could expose the S-rich sublayers to aqueous solutions, promoting periodic flushes of acidic drainage waters (Pratt et al., 1994b). A number of authors believe, on the contrary, that the metal-depleted layers are responsible for passivation of pyrrhotite and other mineral sulfides in nonoxidative and oxidative dissolution reactions (Nicol and Scott, 1979; Buckley and Woods, 1985b; Thomas et al., 1998, 2001; Mikhlin, 2000; Mikhlin et al., 2000, 2001).

Observations of the mineral zoning of oxidized ore deposits, estuarine sediments, and so forth have suggested that pyrite and marcasite are products of pyrrhotite transformations (Burns and Fisher, 1990; Nicholson and Scharer, 1994, and references therein). Burns and Fisher (1990) examined pyrrhotite Fe_7S_8 exposed to sulfuric acid solutions (pH 2) with and without addition of ferric sulfate to simulate deep-weathering processes. They used MS to identify an amorphous phase composed of low-spin ferrous iron akin to pyrite or marcasite, goethite (α-FeOOH), and possibly jarosite. Matsuo et al. (2000) detected by MS and extended X-ray absorption spectroscopy pyrrhotite and then pyrite-type iron sulfide produced during an incubation experiment with sulfate-reducing bacteria. However, there is still a lack of evidence that the amorphous iron-deficient phase converts into crystalline pyrite or marcasite. In recent years, metastable amorphous or poorly crystalline iron monosulfides have attracted a large degree of attention as precursor phases to pyrite formation (Schoonen and Barnes, 1991a, 1991b; Benning et al., 2000; Cahill et al., 2000). Wilkin and Barnes (1996) demonstrated that pyrite forms from mackinawite, Fe_9S_8, and greigite, Fe_3S_4, in slightly oxidative aqueous solutions via loss of iron from rather than addition of sulfur to the precursor monosulfides. On the other hand, Boursiquot et al. (2001) studied the dry oxidation of mackinawite exposed to the air up to 6 months and identified elemental sulfur, iron oxyhydroxides (magnetite and possibly goethite), and intermediate greigite, but not pyrite, as reaction products.

Surface reactivity and composition of iron sulfides is of interest in several other fields, including precipitation of gold and other metals in ore-depositing hydrothermal systems (Widler and Seward, 2002), mineral flotation (Buckley and Woods, 1985a, 1985b; Woods, 1988), hydrometallurgy (Timoshenko et al., 1991; Thomas et al., 1998, 2001), and photovoltaic and high-energy batteries (Thomas et al., 1999; Shao-Horn and Horn, 2001).

The above-mentioned facts show that complex relations in the system Fe-S-O and mechanisms for the reactions involved still need to be understood. The objective of this contribution is to gain deeper insight into pathways of the pyrrhotite transformations under weathering conditions. X-ray powder diffraction and a set of spectroscopic techniques have been employed to document alterations of the nonstoichiometric, strongly iron-deficient layer and products of the NL decomposition that occur during oxidation of acid-reacted pyrrhotites in dry and humid atmospheres at ambient temperature for several months. These systems simulate the behavior of the minerals in zones with changeable water regimes, including gangue pyrrhotite, which was treated in mineral processing and hydrometallurgical processes, in the tailings of concentrating mills and metallurgical plants. The dissimilarity between the behavior of monoclinic and hexagonal pyrrhotites also was under consideration.

2. EXPERIMENTAL

2.1. Materials, Leaching, and Aging Experiments

Natural monoclinic pyrrhotite (Fe_7S_8) used in the experiments was of unknown origin; X-ray powder diffraction analysis and MS showed that the mineral had no impurities excepting 1 to 3% mass of quartz (see below). Hexagonal pyrrhotite, Fe_9S_{10}, from the Norilsk ore deposit (Russia) included pentlandite, $(Fe,Ni)_9S_8$ (impurity 1 to 4%); it has been described in detail elsewhere (Mikhlin et al., 1995, 1998). The specimens were ground in air to approximately 60 μm in particle size and then leached in 1 mol/L HCl in a water-jacket glass vessel at 50°C for 1 h. The slurries (10% solid) were agitated by an overhead stirrer, and no attempt was made to prevent ingress of air and to flush the H_2S produced. The H_2S evolution from a hexagonal mineral started after 3 to 5 min, while no induction period was observed for the dissolution of monoclinic pyrrhotite. The conditioning in solution of hydrochloric acid but not sulfuric acid was chosen to avoid problems related with the presence of lines of sulfate adsorbed from the H_2SO_4 solution in XPS and Fourier transform infrared (FTIR) spectra. The effect of acid anion on the NL composition seems to take place. Pratt and Nesbitt (1997) reported different AES depth profiles for pyrrhotite surfaces reacted in the acid mixtures with various Cl^-/SO_4^{2-} ratios, but several experiments in the current work revealed only minor differences between the spectra of samples treated with hydrochloric and sulfuric acid solutions.

The leaching residue of approximately 40% mass of the initial sample was quickly washed with fresh, cold hydrochloric acid solution and then with water at a paper filter under vacuum. A portion of the wet sample was transferred into the vacuum chamber of an X-ray photoelectron spectrometer or was hermetically sealed in a plastic bag and transported into a Mössbauer spectrometer or an electron paramagnetic resonance (EPR) spectrometer; another portion was dried in air at ambient temperature before FTIR spectroscopy and XRD experiments. The major share of the residue was divided into two parts, which were stored in a desiccator (with periodic access for laboratory air) at 20 ± 2°C either above silica gel at approximately 10% relative humidity or above a water mirror at 100% relative humidity. Portions of the "dry" and "wet" samples were withdrawn at predetermined times up to 5 months and characterized, within 10 to 60 min after extraction, by the spectroscopic techniques and XRD. The "wet" specimens contained, according to thermal analysis, ~10% of free moisture, and they were allowed to desiccate in the atmosphere immediately before the XRD and FTIR spectroscopy examinations.

2.2. Instrumentation and Data Analysis

X-ray powder diffraction patterns were registered using a DRON-4 instrument and monochromatic Cu Kα irradiation. Infrared spectra were obtained via transmission in KBr pellets (spectral degree in purity) using a Vector-22 Fourier transform spectrometer (Bruker). The spectra normalized to the specimen mass are the result of subtracting of the KBr spectrum from those of the mixture pellets. A few experiments carried out by the attenuated total reflection method with ZnSe crystal as a reflection element showed essentially the same results. EPR spectra were recorded at both room temperature and 78 K using an RE 13307 X-band spectrometer (Tesla) applying 100 kHz modulation with a resonance frequency of 9.0 GHz. X-ray photoelectron spectra were acquired using an X-ray photoelectron spectrometer (VG Microtech) at room temperature. The C 1s peak of the hydrocarbon contamination at 285.0 eV was used to correct the binding energies for charging. A nonlinear background subtraction and a Gaussian-Lorentzian model were employed to analyze the spectra; the device, analytical conditions, and data processing procedure were identical to those described previously (Mikhlin et al., 1998, 2000). X-ray fluorescent emission spectra were collected at 78 K using a spectrometer (Stearat) equipped with an X-ray tube with a copper anode, a gas flow proportional detector, and a single crystal of rubidium biftalate (2d = 2.621 nm). Transmission Mössbauer spectra were measured using an NP-610 spectrometer with a ^{57}Co(Pd) source of γ-photons at ambient temperature; the velocity calibration was performed with respect to α-Fe.

3. RESULTS

3.1. XRD

Figure 1 illustrates the XRD patterns of intrinsic monoclinic pyrrhotite, the mineral leached in the hydrochloric acid solution, and samples leached and then aged in the dry and moist environments. After the leaching, intensities of pyrrhotite reflections decreased about 5 times, but their ratios and positions did not change (Fig. 1b), indicating that a reaction product was amorphous and the structure of buried pyrrhotite remained undistorted. The acid-treated sample also exhibited new reflections consistent with orthorhombic α-sulfur at 0.385, 0.344, 0.333, 0.321, and 0.311 nm (Powder Diffraction File, card 17-200). Very similar results were obtained previously for hexagonal pyrrhotite (Mikhlin et al., 1995). The quantity of sulfur slightly increased for the specimens aged over 5 months in dry air (Figs. 1c to 1e), but it grew essentially faster at 100% humidity (Figs. 1f to 1h). The samples exposed to the humid atmosphere additionally showed reflections corresponding to goethite, α-FeOOH (Powder Diffraction File, card 21-1066). The peak at 0.334 nm, which overlaps weak reflections from pyrrhotite and α-sulfur, and the peak at 0.426 nm appear to have arisen from an adventitious impurity of quartz (Powder Diffraction File, card 33-1161). Few additional reflections could not be assigned to any known compounds of iron, sulfur, and oxygen. In all cases, the intensities of the pyrrhotite peaks did not decrease during the aging, suggesting that sulfur and goethite were produced by decomposition of the amorphous phase.

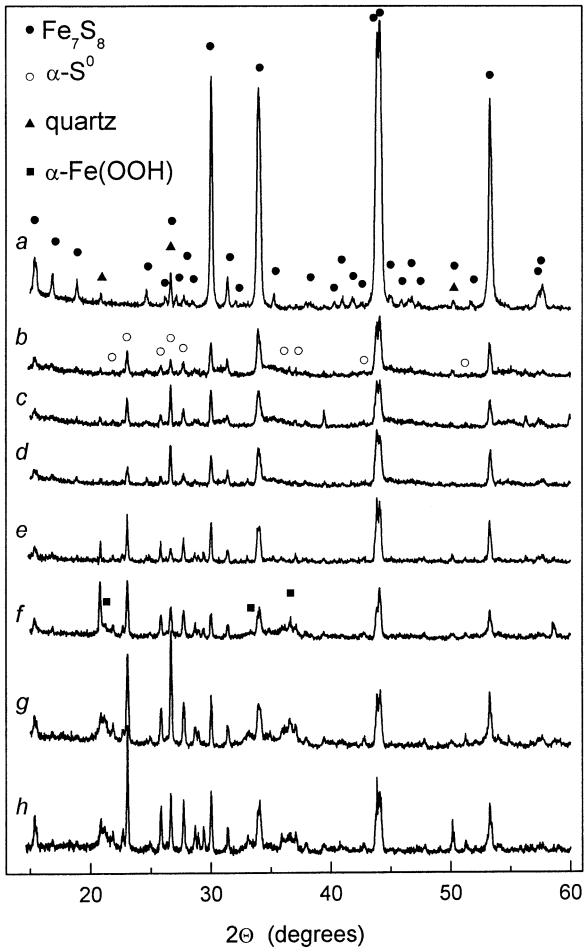

Fig. 1. X-ray powder diffraction patterns of monoclinic pyrrhotite samples (a) before and (b) after 1 mol/L HCl leaching; after acidic treatment and aging in dry air for (c) 8 d, (d) 23 d, (e) 150 d; and after acidic treatment and aging in humid air for (f) 7 d, (g) 23 d, and (h) 150 d.

3.2. Infrared Spectroscopy

Representative FTIR spectra of reacted hexagonal and monoclinic pyrrhotite samples are shown in Figure 2. The spectrum of pyrrhotite air oxidized at ambient temperature for several months contains weak lines of stretching vibrations of OH groups centered at ~3230 cm^{-1} and of vibrations located in the range of 400 to 1300 cm^{-1} (Fig. 2a). The pyrrhotite samples leached and quickly dehydrated at 20°C display a much more intense band of the OH stretching vibrations at 3420 to 3500 cm^{-1} and a shoulder at approximately 3270 cm^{-1} (Fig. 2b). The high-frequency components of the band may be associated with surface H_2O and OH groups, while the lines at the lower

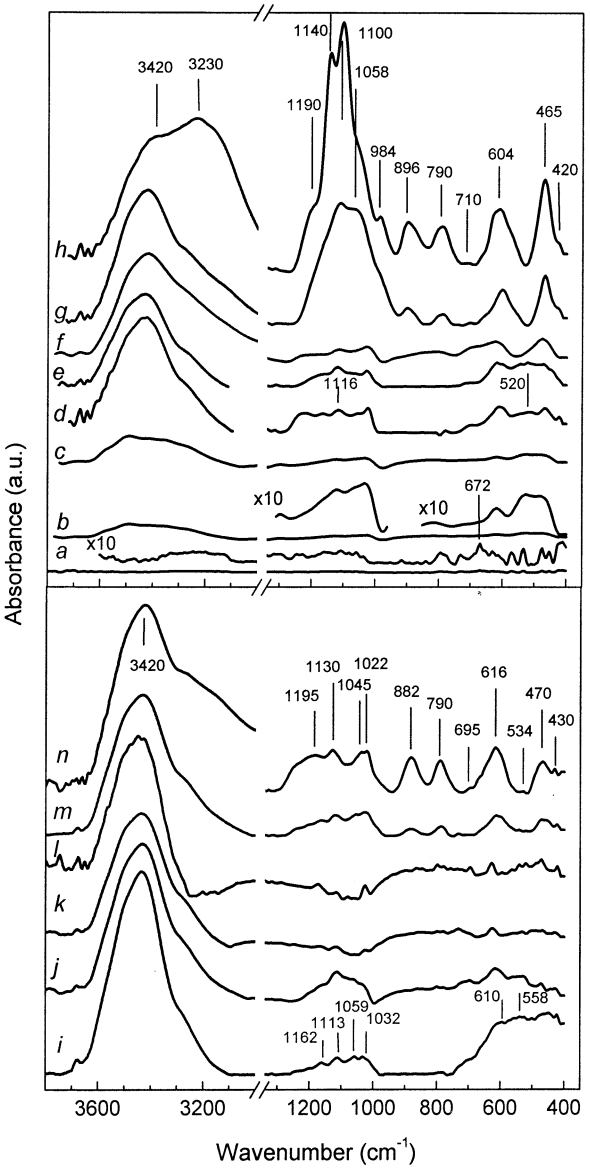

Fig. 2. Fourier transform infrared absorption spectra of hexagonal pyrrhotite (a) oxidized in air for 150 d; (b) ground and leached in 1 mol/L HCl; leached and aged in dry air for (c) 1 d, (d) 15 d, (e) 60 d; leached and aged in humid air for (f) 1 d, (g) 5 d, (h) 30 d; and of monoclinic pyrrhotite (i) leached in 1 mol/L HCl; (j) leached and heated in dry air at 150°C for 30 min; leached and aged in dry air for (k) 7 d, (l) 60 d; and leached and aged in humid air for (m) 7 d and (n) 20 d.

wave numbers appear to have originated from the species involved in stronger interactions, in particular from bulk OH in iron oxyhydroxides (Tejedor-Tejedor and Anderson, 1986). The band increased during 4 weeks of aging in dry air and then slowly diminished, but the low-frequency shoulder grew steadily in the case of the samples exposed to the humid environment. The H_2O-bending band at 1630 cm^{-1} is considerably weaker than the stretching bands. A broad line at wave numbers <800 cm^{-1} that varies in the same way as the above H_2O bands seems to correspond to adsorbed water (Nakamoto, 1986). These facts imply an extension of hydrophilic surfaces of the specimens, probably because of partial decay of the NL and formation of fine hydrophilic particles, and a subsequent coarsening of the particles. The intensity of the OH vibrations is higher for the samples of monoclinic pyrrhotite than of hexagonal pyrrhotite, with the differences being most strongly marked at the early stages of the NL degradation.

The leaching also gave rise to a variety of narrow lines in the range of 1200 to 400 cm^{-1}. For the samples of hexagonal pyrrhotite aged in dry air, the band intensities increased for ~15 d and then slightly reduced. Monoclinic pyrrhotite behaved similarly, although the freshly leached samples showed a stronger absorption and somewhat different shapes of the bands. A specimen dehydrated at 150°C for 30 min has a spectrum resembling that of the sample aged at low humidity, but the intensities of the lines at 1113, 1030 and 615 cm^{-1} are commonly higher (Fig. 2j). The band(s) falling in the region of 520 to 570 cm^{-1} for the "dry" samples almost disappear for the "wet" ones and can be attributed to amorphous or poorly crystalline iron oxides (Nowok and Stenberg, 1988). Several distinct bands arose in the spectra after the leached samples were exposed to the humid air. A couple of lines at 890 and 790 cm^{-1} certainly correspond to Fe-O-Fe oxy-bridging vibrations and/or Fe-O-H bending vibrations of goethite (Tejedor-Tejedor and Anderson, 1986). Some other peaks also could have originated from ferric oxyhydroxides (Brienne et al., 1994, Murad and Bishop, 2000), but in all likelihood, they are associated with sulfoxy species.

Free sulfate ions are known to exhibit two bands responding to υ_3 and υ_4 vibrations at ~1100 and 610 cm^{-1}, while vibrations υ_1 at ~980 cm^{-1} and υ_2 at ~450 cm^{-1} are forbidden in infrared spectra (Nakamoto, 1986). When the tetrahedral SO_4^{2-} ion is distorted because of a coordination to metal and hydrogen ions, the bands υ_3 and υ_4 are split and shifted, and the υ_1 and υ_2 modes become active. Consequently, the peaks or shoulders at 1130 to 1140, 1020 to 1030, 980, 610, and 470 cm^{-1} are attributable to sulfate in monodentate coordination to Fe(III) (C_{3v} symmetry), and an additional peak at ~1200 cm^{-1} may be due to bidentate coordination (C_{2v} symmetry) (Eggleston et al., 1998). On the other hand, the appearance of a band at or above 1190 to 1200 cm^{-1} may reflect the formation of adsorbed bisulfate or sulfate-H_3O^+ structure (Persson and Lövgren, 1996; Eggleston et al., 1998). This analysis suggests that a mixture of sulfate and bisulfate ions is formed in the systems under investigation. A share of sulfate in the bidentate coordination to iron and/or of the HSO_4^- ions is higher in the case of monoclinic pyrrhotite, whereas a relative quantity of free SO_4^{2-} (in fact, probably, an outer-sphere ligand in the second shell) is larger for the hexagonal pyrrhotite samples, but this is still arguable. Moreover, sulfite SO_3^{2-} and thiosulfate $S_2O_3^{2-}$ display lines in the same spectral intervals, with the frequencies depending on a binding mode. In particular, the asymmetric and symmetric S-O stretches were observed at 1115 and 996 cm^{-1} for thiosulfate coordinated to a metal via oxygen (Degenhardt and McQuillan, 1999), they should be shifted to higher energies when $S_2O_3^{2-}$ or SO_3^{2-} coordinate metal via sulfur (Nakamoto, 1986). Therefore, some maxima could be assigned to thiosulfate or other S-O species, especially at early stages of the ageing and for the "dry" samples.

The peaks at 420 to 430 and, possibly, 460 to 470 cm^{-1} can be related with elemental sulfur, polysulfide, and disulfide

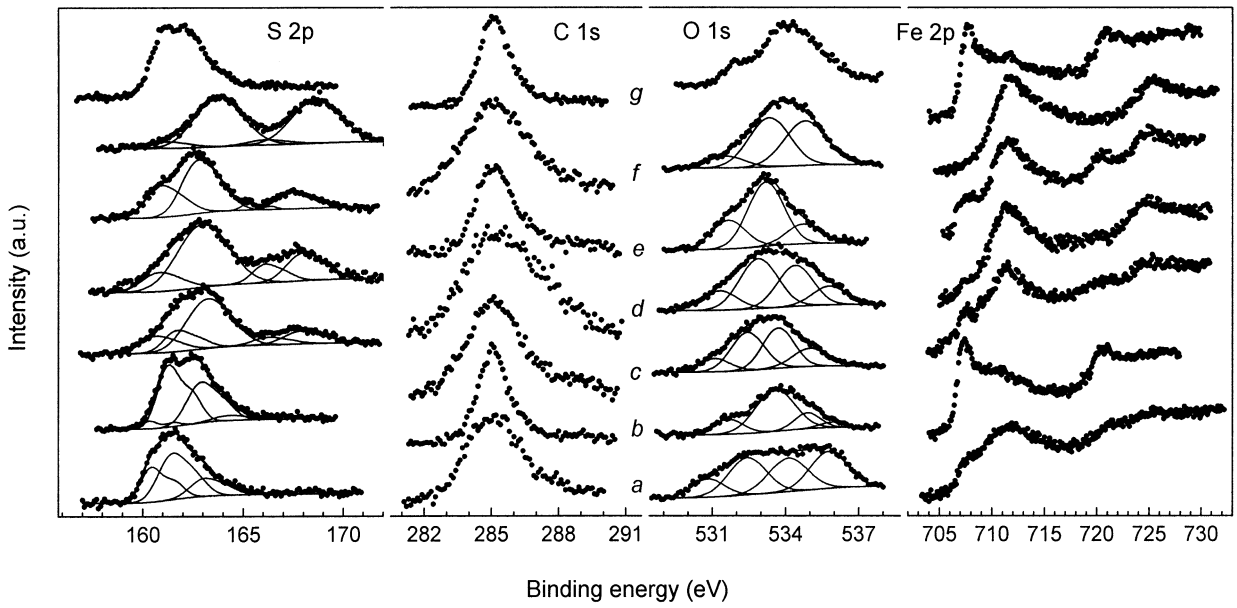

Fig. 3. X-ray photoelectron spectra S 2p, C 1s, O 1s, Fe 2p of monoclinic pyrrhotite (a) ground in air; (b) leached in 1 mol/L HCl; leached and aged in dry air for (c) 7 d and (d) 28 d; leached and aged in humid air for (e) 7 d and (f) 28 d; and (g) leached and kept in ultrahigh vacuum for 28 d. The spectra are normalized to maximum height.

species, although S-S vibrations are active only in Raman spectra (Mycroft et al., 1990; Toniazzo et al., 1999; El Jaroudi et al., 1999). A comparison between the FTIR spectroscopy, XPS, and XRD data implies that all the infrared responses come from the NL degradation products and adsorbed species rather than from the nonstoichiometric layer itself.

3.3. XPS

The X-ray photoelectron S 2p spectrum of monoclinic pyrrhotite ground in air shows the presence of monosulfide at a binding energy (BE) of 160.5 eV, disulfide at 161.6 eV, and minor polysulfide species at ~163.3 eV (Fig. 3a). The Fe 2p spectrum includes contributions from sulfur-bonded Fe(II) at ~707.5 eV, oxygen-bonded ferric iron at ~711 eV, and possibly Fe(II)-O and Fe(III)-S species at 708 to 709 eV, with all of them composed of several multiplet lines (Pratt et al., 1994a). Fitting the Fe 2p spectra is not, in our opinion, unequivocal and is omitted in Figure 3. The O 1s band is surprisingly wide, suggesting a nonuniform electrostatic charging of the surface layer, because the C 1s, Fe 2p, and possibly S 2p lines of the air-oxidized pyrrhotite are very broad too. The spectrum is expected to represent O^{2-} species (~530 eV), hydroxide groups (~531 eV), and chemically (~532 eV) and physically (533 to 535 eV) attached water, but the inhomogeneous charging of sulfide and oxyhydroxide phases and possibly carbonaceous film, along with differences in chemical shifts for various phases, may affect the line widths and positions.

The S 2p spectrum of pyrrhotite leached in acid (Fig. 3b) exhibits an enhanced polysulfide line and a reduced one of monosulfide. Surface elemental sulfur (BE = ~164 eV) is known to evaporate in the ultrahigh vacuum at room temperature, but the bulk substance, whose abundance is confirmed by XRD, can contribute to the spectra. A weak line at 164.5 eV corresponds to a reaction product consisting of a sulfur species of intermediate (+1 or +2) oxidation state (Schaufuß et al., 1998a, 1998b). The narrow peak at 707.4 eV that dominates the Fe 2p spectrum should be assigned to singlet Fe(II) (Mikhlin et al., 1998, 2000; see also the next section), but different iron species are present as well. The total concentration of the surface iron is decreased, and the atomic S/Fe ratio reaches 2.2 (Table 1). The oxygen content reduces relative to air-ground mineral but is higher than that of leached hexagonal pyrrhotites (Mikhlin et al., 1998, 2000); the prevailing oxygen-bearing species is water. The C 1s spectrum becomes noticeably narrower, suggesting a rather uniform surface.

The broadening progresses with time of aging, most evidently for S 2p and C 1s bands, and is more rapid for "dry" specimens, although the oxidation is faster at 100% humidity. All the components of the spectra (i.e., those corresponding to sulfide, sulfoxy species, etc.) widen about equally, so the phenomenon relates with nonuniform electrostatic charging rather than with the multiphase composition of the substrate. At the same time, the fits in Figure 4 are fairly approximate because the broadening complicates data processing. The Fe 2p spectra show a gradual reduction of the low-spin Fe(II) peak at 707.5

Table 1. Surface atomic ratios determined from the X-ray photoelectron spectra of monoclinic pyrrhotite.

Sample	S/Fe	O/Fe	C/Fe
Ground in air	1.4	3.2	3.6
Leached in 1 mol/L HCl for 1 h	2.2	1.7	5.8
And then aged in dry air for 7 d	3.1	5.6	6.3
In dry air for 28 d	2.4	4.6	4.3
In humid air for 7 d	2.2	7.2	5.0
In humid air for 28 d	1.8	5.8	3.5
In a vacuum for 28 d	2.5	2.8	10

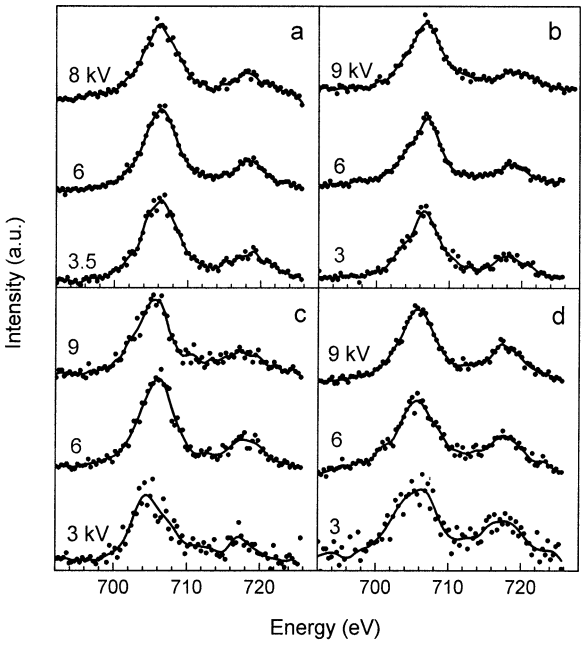

Fig. 4. X-ray Fe Lα,β emission spectra of monoclinic pyrrhotite plates (a) abraded in air, (b) leached in 1 mol/L HCl for 1 h, and leached and aged in (c) dry air and (d) humid air for 7 d. The numbers near the curves stand for the accelerating voltages at the X-ray tube.

eV and an enlargement of the Fe(III)-O contribution at ~711 eV, with the changes for the "dry" samples being slower than for the "wet" ones. The air oxidation for 7 d results in an increase in the relative concentrations of monosulfide, polysulfide, and, possibly, elemental sulfur. Earlier (Mikhlin et al., 2000), the "disulfide" lines were suggested to attribute, aside from S_2^{2-} groups, to the end atoms of polysulfide chains, which are known to possess more negative charge than the intermediate atoms. Therefore, the alterations may be interpreted as the growth of the polysulfide clusters, right to elemental sulfur S_8, yielding concurrently some amount of monosulfide species. The higher BE peaks, whose intensities increase throughout the aging and are lesser for the "dry" samples, are better fitted with two S 2p doublets attributable to a series of sulfoxy species. Schaufuß et al. (1998a, 1998b) reported very similar S 2p spectra of air-oxidized pyrite. In the high-resolution spectra excited by synchrotron irradiation, the authors specified components at 168.3, 167.4, and 166.4 eV and assigned them to sulfate, thiosulfate, and sulfite, respectively. These lines may occur in the spectra in Figure 3 too, but the presence of sulfate is quite definite only for the "wet" specimens aged for 4 weeks.

The S/Fe ratio increases after the NL oxidation in dry air for 7 d and remains nearly constant in the wet medium (Table 1). This signifies an additional enrichment of the sulfide phase in sulfur, provided that the ferric oxyhydroxides and sulfoxy salts are irregular distributed over the surface. A subsequent decrease in the S/Fe ratio is caused by further formation of the oxidized products, which screen the sulfide surface, and the probable incorporation of oxygen into the NL. The amount of oxygen increases by a factor of 3 to 4 as a result of the aging.

The acid-treated pyrrhotite held in the ultrahigh vacuum for 28 d shows an increase in carbon and oxygen contents caused by H_2O and carbonaceous contaminations. The S 2p band shape and the S/Fe ratio do not vary, indicating a very low volatility of the over-stoichiometric sulfur.

3.4. X-ray Emission Spectroscopy

In contrast to XPS, soft X-ray fluorescent emission spectroscopy (XES) characterizes a subsurface layer, the thickness of which can be varied from few nanometers to several hundreds of nanometers by changing the X-ray tube accelerating voltage, with a higher voltage corresponding to a thicker probing layer (Galakhov and Kurmaev, 1987; Mikhlin et al., 2000). The Fe Lα,β emission spectra arise from Fe 3d4s $\rightarrow$ 2p electron transitions, and the line shape provides information on the local partial density of the occupied Fe 3d states mainly. The Fe Lβ/Lα peak ratio is sensitive to the chemical state of iron; in particular, it is lower for singlet Fe(II) and Fe(III) species than for high-spin Fe(II) (Soezima et al., 1978; Laputina, 1991).

The spectrum of acid-leached monoclinic pyrrhotite differs from that of unreacted mineral in the reduced Lβ/Lα ratio (0.28 $\pm$ 0.02 vs. 0.33), the peak energy (increased by ~0.6 eV), and the Fe Lα band shape (Figs. 4a and 4b). This is consistent with a model of the NL electronic structure, according to which the $2t_{2g}$ level of singlet Fe(II) is located in the upper portion of the valence band formed by nonbonding orbitals of polysulfides (Mikhlin et al., 1998). The shoulder at ~704 eV is associated with an admixture of the Fe 3d states to the states of S-S species, although additional forms of iron could be also involved. After the samples have been aged in a dry atmosphere, the peak energy is decreased by almost 1 eV, the Lβ/Lα ratio is 0.30, and the low-energy shoulder is seen only at the highest accelerating voltages used (i.e., for the largest depths analyzed; Fig. 4c). This can be explained in terms of the transformation, maybe partial, of the low-spin Fe(II) to Fe(III) within the outer strata of the NL. For the samples exposed to the wet environment, the line becomes broader, and the Lβ/Lα ratio approaches 0.50 (Fig. 4d). This value is higher than that for intrinsic pyrrhotite, suggesting a presence of quintet Fe(II) bonded with oxygen and/or sulfoxy species instead of sulfur (Soezima et al., 1978; Galakhov and Kurmaev, 1987; Laputina, 1991). The spectra acquired at the lowest accelerating voltage of 3 kV are heavily affected by the surface oxidation and could be attributed to predominant Fe(III) species. The high-spin ferrous iron is therefore an intermediate product of the singlet Fe(II)-to-Fe(III) conversion in the humid environment, whereas the reaction seems to proceed directly at low relative humidity.

3.5. MS

The Mössbauer spectra of monoclinic pyrrhotite show a prominent signal with an isomer shift of $\delta = 0.36$ mm/s arising as a result of the acidic leaching and aging (Fig. 5); the intensity of the signal corresponds to >50% total iron. The lines of monoclinic pyrrhotite do not change, and aside from the above, no additional features appear. Very similar behavior was reported for the MS of acid-leached hexagonal pyrrhotites (Mikhlin et al., 1995, 2000). The central parts of the spectra measured over an extended velocity scale are shown in Figures 5c to 5k. The new band in the spectrum of the "wet" sample

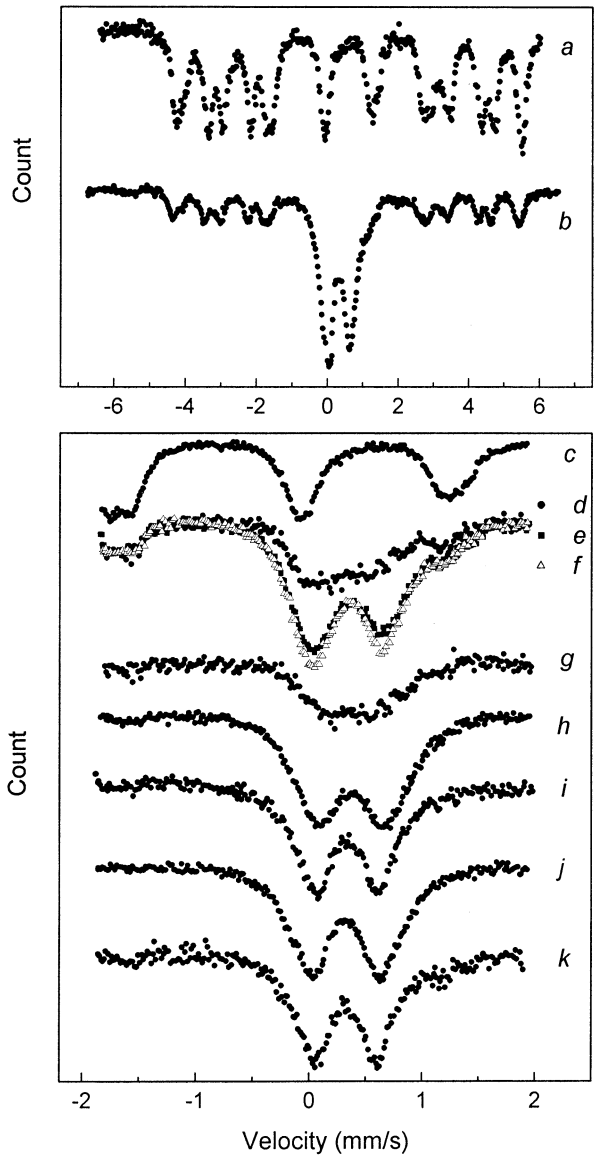

Fig. 5. Mössbauer spectra of monoclinic pyrrhotite (a) ground in air and (b) leached in 1 mol/L HCl and then stored in dry air for 28 d; (c) the central portions of the spectra of the mineral ground in air, (d) the same specimen leached in 1 mol/L HCl and then aged in dry air for (e) 3 d and (f) 5 d; difference spectra of the samples (g) leached, (h) leached and aged in dry air for 3 d, (i) in humid air for 7 d, (j) in dry air for 22 d, (h) in humid air for 22 d, and (c) the sample.

measured immediately after the leaching is broad and almost unsplit; the XPS and XES results (Figs. 3 and 4) testify that it corresponds to the dominant low-spin ferrous iron and some amount of paramagnetic ferric iron in the metal-depleted layer (Mikhlin et al., 1995, 2000). The air aging, under both dry and humid conditions, leads to an increase in the intensity and quadrupole splitting ϵ of the signal, while the isomer shift remains constant. The ϵ value approaches 0.62 mm/s, suggesting a distortion of the low-spin Fe(II) environment and/or a decrease in electron density at the iron nuclei and is somewhat higher for "dry" specimens. No discernible quintet ferrous iron differing from that of initial pyrrhotite has been detected, so the quantity of this species found by XES is insignificant. Boursiquot et al. (2001) have recently reported a Mössbauer spectrum of mackinawite resembling the NL spectra and have fitted that with one singlet (δ = 0.42 mm/s) and two doublets (δ = 0.13 nm/s, δ = 0.38 mm/s , and δ = 0.41; ϵ = 0.64 mm/s). These lines were interpreted as low-spin Fe(II) in sites with no Fe(III) as the nearest neighbor, Fe(III), and Fe(II) atoms with Fe(III) as the nearest neighbor, respectively. If this concept is valid, the parameters of the spectra illustrated in Figure 5 mean that the low-spin Fe(II) is gradually oxidized to Fe(III) within the NL, in qualitative agreement with XES and EPR data.

One can see from the d, e, and f spectra in Figure 5 that the quantity of iron atoms contributing to the NL spectrum increases with time of aging. This should be related with a γ-resonance probability, that is, the fraction of ^{57}Fe atoms able to absorb the nuclear recoil energy and undergo the Mössbauer effect, since the lines of unaltered pyrrhotite do not change. The vibrational amplitudes of the ^{57}Fe nucleus are known to play a major role in determining this value. Therefore, the low probability is due to a "mild" atomic structure of the disordered NL produced by the leaching. Subsequent oxidation induces the conversion of the structure to a more rigid one simultaneously with the partial Fe(II)-to-Fe(III) transformation and, perhaps, incorporation of oxygen. No lines attributable to goethite, ferric sulfate, and so on are seen in the spectra. Amorphous or nanocrystalline, and hence superparamagnetic, goethite and other products of the NL decomposition may contribute to the band in the central part of the room-temperature spectra (Burns and Fisher, 1990; Boursiquot et al., 2001), but it is difficult to distinguish these phases, especially because their quantities are minor (see above).

3.6. EPR

Neither unpaired spins of electrons localized at plentiful defect sites in the amorphous NL ($g \sim 1$) nor paramagnetic ferric iron (g = 3 to 3.5) has been found for the acid-reacted pyrrhotite samples, although very weak signals of Fe(III) species are detectable for air-ground minerals (Fig. 6). The absence of unpaired localized electrons was proposed to explain on the basis of a similarity between the NL and noncrystalline chalcogens and chalcogenides (Mikhlin, 2000). In these materials, electronic levels of the defect centers with negative correlation energy, mostly lone pair p-orbitals of chalcogen atoms, are either occupied by two electrons or empty (Kastner et al., 1976; Mott and Davis, 1979; Tsendin et al., 1996). The EPR signal corresponding to ferric iron is believed to be very broad because of a fast electron exchange between Fe sites. Consequently, no characteristic Fe(III) signals are observed in the spectra of the samples aged for $<$45 d (Figs. 6c to 6d). After the specimens have been exposed to the dry atmosphere for 49 d and to the humid atmosphere for $>$90 d, a series of narrow lines of paramagnetic Fe(III) species emerge (Figs. 6e to 6h). The turning of the samples in the spectrometer displaces the narrow lines in a scale of the magnetic field, probably because of an anisotropy and misalignment of nanometer-scale phases and/or spatially separated regions containing dominant Fe(III) ions. Several wide bands are thought to originate from larger crystals of goethite and other substances; the spectra, however, appear

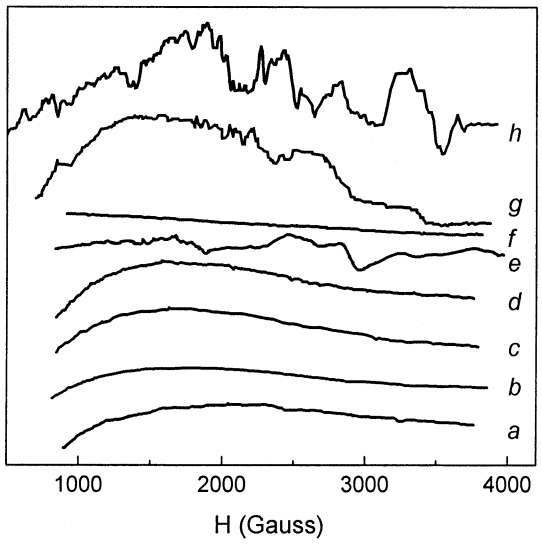

Fig. 6. Electron paramagnetic resonance spectra of monoclinic pyrrhotite specimens (a) air-ground, (b) leached in 1 mol/L HCl, leached and aged in (c) dry air and (d) humid air for 18 d, in (e) dry air and (f) humid air for 49 d, and in (g) dry air and (h) humid air for 150 d.

rather complex for interpretation. The late appearance of a response from the ferric oxyhydroxide and sulfoxy phases suggests that they are involved, together with the NL, with the fast electronic exchange.

4. DISCUSSION

4.1. Products of NL Degradation

The results obtained by various techniques for monoclinic pyrrhotite are briefly summarized in Table 2. It is worth noting that the XRD, FTIR spectroscopy, and probably EPR data are related to products of the nonequilibrium layer decomposition; MS and XES characterize mainly the bulky NL; and XPS describes surface layers of the solid products and adsorbed species. Elemental sulfur is the major sulfur-bearing end product of the NL destruction and the only crystalline one. FTIR spectroscopy and XPS have revealed also sulfate that appears to be present as amorphous ferric iron basic sulfates and adsorbed SO_4^{2-} and HSO_4^- ions. Other sulfoxy species detected by XPS, such as sulfite (BE = ~166.3 eV), whose surface concentration is higher for the "dry" specimens, thiosulfate (BE = ~167.6 eV), existing probably in the "wet" specimens, and various polythionates are intermediates and do not accumulate over the aging. Goethite, probably nanocrystalline, is confidently recognized both by XRD and FTIR spectroscopy in the samples exposed to the moist medium, whereas an unidentified ferric oxide is found in the experiments at low humidity. The apparent difference between monoclinic and hexagonal pyrrhotites is the larger quantity of OH groups and attached H_2O for the former, but this distinction vanishes after rather prolonged aging. It is interesting, however, that the FTIR spectroscopy data point to a lower ratio of goethite to sulfate formed in the case of hexagonal pyrrhotite. This may mean a lesser quantity of acid released because of Fe(OOH) formation (Murad et al., 1994). Pyrite, greigite, pyrrhotite, or other iron sulfides do not crystallize from the amorphous metal-deficient phase. Also, there are no signs that the pyrrhotites buried under the NLs after the acidic leaching undergo any further alterations throughout the aging.

It is not surprising that the oxidation of the iron-deficient layers of the acid-reacted pyrrhotites proceeds much more rapidly than of initial, unleached minerals, and that the NL decay at 100% relative humidity is much faster than at low humidity, although the layer becomes more disordered in the dry air. The products of all these reactions are similar in the main (Nicholson and Scharer, 1994; Pratt et al., 1994a,b). These facts suggest a so-called polysulfide reaction pathway for pyrrhotite oxidation. That is, the preferential release of sulfidic

Table 2. Summary of the results obtained for the air degradation of acid-reacted monoclinic pyrrhotite.

	Method used					
Sample	XRD	FTIR spectroscopy	XPS	XES	MS	EPR
Monoclinic pyrrhotite leached in 1 mol/L HCl	α-S^0	OH, minor S-O, S-S (?), Fe-OH species	S^{2-}, S_n^{2}, singlet Fe(II), minor Fe(III)-O species	Singlet Fe(II)	Singlet Fe(II), low probability of γ-resonance	No unpaired spins
Leached and aged in dry air	α-S^0	OH, minor SO_4^{2-}, S-O, Fe_2O_3(?), S-S species (?)	S^{2-}, S_n^{2-}, SO_3^{2-}, $S_xO_y^{2-}$, SO_4^{2-}, Fe(III)-O species, minor singlet Fe(II)	Singlet Fe(II), Fe(III)	Singlet Fe(II), paramagnetic Fe(III)	Fe(III) species after aging for 49 d
Leached and aged in humid air	α-S^0, goethite	OH, $FeSO_4^+$, HSO_4^-, goethite, S-S species (?)	S_n^{2-}, S^0, SO_4^{2-}, SO_3^{2-}, $S_xO_y^{2-}$, Fe(III)-O species	Quintet Fe(II)	Singlet Fe(II), paramagnetic Fe(III)	Fe(III) species after aging for 90 d

EPR = electron paramagnetic resonance, FTIR = Fourier transform infrared, MS = Mössbauer spectroscopy, XES = X-ray emission spectroscopy, XPS = X-ray photoelectron spectroscopy, XRD = X-ray diffraction.

iron into oxyhydroxide or aqueous phase causes the deficiency of iron, and then S-S bonding eliminates the excessive anionic valences. However, further growth of polysulfide ions and Fe(II)-to-Fe(III) transition in the course of the air oxidation are possible only if additional anions, particularly oxygen species, are included in the solid. A large number of structural vacancies in the metal-depleted layer are thought to allow oxygen diffusion to the interior. The Auger depth profiles (Pratt et al., 1994a,b; 1997), bulk chemical analysis (Mikhlin et al., 1995) and X-ray emission O K spectra (Mikhlin et al., 2000) of pyrrhotites acid reacted and then exposed to air support this assumption. The concentration, distribution, and chemical state of oxygen cannot be directly determined by the techniques used in the current study, though XPS and FTIR spectroscopy data seem to be indicative of primarily OH groups. One can see that the nonstoichiometric structure formed is rather stable, and considerable solid-state alterations precede its destruction, which yields S^0, α-FeOOH, and so on afterward. This evolution should substantially affect the mineral reactivity and reflect mechanisms for the reactions involved.

4.2. Solid-State Reactions Within the NL

The reduced intensity of the Mössbauer spectra and the absence of an EPR signal from unpaired electrons provide evidence of a "mild" lattice of the NL, which facilitates atomic rearrangements. The mechanism for sulfur-sulfur interactions on the basis of the concepts accepted in the physics of noncrystalline chalcogens (Kastner et al., 1976; Mott and Davis, 1979; Tsendin et al., 1996) was developed earlier (Mikhlin, 2000). In brief, the end atoms of the polysulfide chains are believed to be the active centers, nonbonding S 3p-type orbitals of which are the highest occupied orbitals in the NL. The removal of a couple of electrons (not a single electron) from these levels produces unstable centers $-S^+$ capable of interacting with negatively charged terminal atoms $-S^-$, thus joining the S-S chains. When there are no more close and mobile enough sites $-S^-$, the $-S^+$ center would bind the intermediate sulfur of S-S clusters, branching the S-S chains. A positively charged atom that is connected with three chalcogen atoms was considered to be a principal donor defect for glassy chalcogens (Kastner et al., 1976), but it seems hardly stable in the NL because of sterical and other factors. Instead, a split of the S-S chains is expected to yield elemental α-sulfur (S_8) along with lower polysulfides:

$$^-S-(S)_m-S^+ + {}^-S-(S)_n-S^- = (S)_{m+n-4}{}^{2-} + S_8. \quad (4)$$

Alternatively, the $-S^+$ centers may coordinate to OH^- ions or promote the formation of Fe(III) ions, especially as the NL structure becomes more rigid and the rates of atomic rearrangement and therefore of S-S bonding fall:

$$^-S-(S)_m-S^+ + OH^- = {}^-S-(S)_m-S-OH, \quad (5)$$

$$^-S-(S)_m-S^+ + 2Fe^{2+} = {}^-S-(S)_m-S^- + 2Fe^{3+}. \quad (6)$$

Further oxidation appears to occur via splitting of the terminal S atoms by the arbitrary reaction:

$$^-S-(S)_m-S-OH + H_2O = {}^-S-(S)_m-S^- + S-(OH)_2{}^- + H^+. \quad (7)$$

Consequently, the output of thiosulfate and sulfate is small if the S-S species are not disulfide. This scheme allows explaining the formation primarily of elemental sulfur as a result of the decomposition of the NL and pyrrhotite itself, in contrast to the large amount of sulfate found after oxidation of pyrite.

Until now, the mechanism of oxidation of iron sulfides has received much more attention in the case of pyrite, although the dominant reaction pathways remain controversial (Lowson, 1982; Luther, 1987; Mishra and Osseo-Asare, 1988; Eggleston et al., 1996; Schaufuß et al., 1998a, 1998b; Kelsall et al., 1999). The mechanistic models have proposed the involvement of intermediary Fe^{2+}-S-S^+-O or S-OH species (Luther, 1987; Schaufuß et al., 1998a, 1998b; Kelsall et al., 1999), Fe^{2+}/Fe^{3+} cycling (Eggleston et al., 1996), and polysulfide pathway (Mycroft et al., 1990; Schaufuß et al., 1998a, 1998b). However, the processes of spin conversion of iron species are largely neglected. Meanwhile, the X-ray emission and EPR results suggest that high-spin Fe(II) plays a major role in the electronic exchange with Fe(III) for periods shorter than characteristic times for Mössbauer and EPR effects (10^{-7} to 10^{-8} s), although the involvement of singlet Fe(II) cannot be ruled out too. Moreover, the reactions occurring via the quintet ferrous iron appear to be more rapid, and the comparison between the NL degradation at low and 100% humidity illustrates this thesis. In addition, Schaufuß et al. (1998a, 1998b) reported that Fe(III)-S sites did not change significantly within the 14-h air oxidation of pyrite, while the number of surface Fe(II) species (high-spin ones, as this is seen from the X-ray photoelectron spectra presented) diminished, producing ferric oxyhydroxide. The high-spin ferrous iron is, hence, more active in the iron sulfide oxidation processes than the Fe(III).

The heavily iron-depleted NL contains, in contrast to intrinsic pyrrhotite, the abundant low-spin ferrous iron; the quintet-to-singlet Fe(II) conversion is a consequence of the presence of polysulfide in place of sulfide ligands and, probably, a reduced Fe-S interatomic distance (Mikhlin et al., 1998). The variety of metal vacancies, Fe(III), and certain sulfur sites make possible the absorption of OH groups during the NL formation and particularly following ageing. Hydroxide ions and especially sulfoxy ligands arisen in Eqn. 5 and 7 promote the low-to-high spin transformation. This sequence of events may be the main reason behind the much faster oxidation of the NL in moist environment than in dry air, where the concentration of incorporated oxygen remains comparably low and the oxidation proceeds via the direct conversion of low-spin Fe(II) to Fe(III). It is worth noting also that some iron ions in pyrrhotites are thought to be in Fe(III) state, thus compensating the excessive negative charge of over-stoichiometric sulfur (Bertaut, 1953; Vaughan and Craig, 1978). Accordingly, the larger oxygen concentration in the NL at monoclinic pyrrhotite Fe_7S_8 in comparison with that at hexagonal Fe_9S_{10} may be due to the higher starting deficiency of iron in Fe_7S_8.

4.3. Implications for Weathering Processes

The composition of the iron-depleted layer that forms at pyrrhotite under both anoxic and oxidative conditions as well

as chemical states of iron and sulfur in the layer resemble those for marcasite and pyrite (see references cited under "Introduction" and the results above). It is known also that pyrite arises from iron monosulfides (mackinawite and greigite) via loss of iron from the solid in aqueous solutions (Wilkin and Barnes, 1996). Furthermore, the process is more rapid if surfaces of the starting sulfides were previously oxidized in air (Benning et al., 2000; Cahill et al., 2000). These facts suggest that the iron-deficient structures may be intermediates of or precursors to pyrite formation. However, the formation of pyrite or marcasite did not occur under the conditions of our experiments. Similarly, pyrite was not produced by the gradual oxidation of mackinawite in air, although the intermediate mixed Fe(II)/Fe(III) valence phase greigite was found (Boursiquot et al., 2001). In light of the above discussion, the absence of pyrite may be rationalized in terms of the oxygen incorporation into the solid phase, which promotes NL transformation via different pathways.

The formation and aging of the iron-deficient layers are expected to change substantially the pyrrhotite reactivity. This may have a significant role in processing of pyrrhotite-bearing ores and oxidation of the sulfide wastes, in particular, in the generation of acid mine drainage. Pratt et al. (1994b) suggested that the passivating Fe(III)-oxyhydroxide coatings, whose uncompromised integrity is maintained under moist conditions, inhibit pyrrhotite oxidation and hence the acid production. The results of the current research show that the oxidation of the NL in the wet environment is rather fast despite occurrence of the oxyhydroxide film. This implies in particular that flooding of the sulfide tailings would not prevent the sulfuric acid runoff. At the same time, it was established that the formation of surface Fe(III)-O species correlates with the passivation of pyrrhotite during electrochemical oxidation in acidic solutions, whereas the thick, strongly iron-depleted layer does not make pyrrhotite passive (Mikhlin et al., 2001). Analyzing the available data, we arrive at the conclusion that the reacted surface layer turns into a passive one because of certain structural alterations. Particularly, the passive structure is strongly nonuniform in terms of random distribution of oxygen, Fe(III), and $-S^{+}$ sites within the disordered and rather rigid lattice (compare with the NL aged in dry air). This may lead to a sharp decrease in the conductivity of the solid (Mott and Davis, 1979; Tsendin et al., 1996) and thus to passivation (Mikhlin et al., 2001). This concept is open to discussion and will be examined in more detail elsewhere.

5. CONCLUSION

The combined XRD and spectroscopic study of the aging of massive, amorphous, metal-depleted, nonequilibrium products formed at pyrrhotites in acids allows us to monitor the evolution of the layer as a spatially expanded reaction zone and to specify the products of iron sulfide oxidation. The measure of "elasticity" of the NL atomic lattice, complex transformation of sulfur species, oxygen incorporation, and alterations of the oxidation and spin state of iron have been established to determine the oxidation kinetics and products, which depend on the environment humidity and differ somewhat for monoclinic and hexagonal pyrrhotites. Pyrite, marcasite, and greigite have been found to not crystallize from the amorphous NL. The passivation of pyrrhotite is due to special properties of the partially oxidized NL rather than the ferric oxyhydroxide coatings.

Acknowledgments—The authors acknowledge financial support from the Russian Foundation for Basic Research, grant 99-03-32562.

Associate editor: E. H. Oelkers

REFERENCES

Benning L. G., Wilkin R. T., and Barnes H. L. (2000) Reaction pathways in the Fe-S system below 100°C. *Chem. Geol.* **167,** 25–51.

Bertaut E. F. (1953) Contribution a l'etude des structures lacunaires: La pyrrhotine. *Acta Crystallogr.* **6,** 557–561.

Blowes D. W. and Jambor J. L. (1990) The pore-water geochemistry and the mineralogy of the vadose zone of sulfide tailings, Waite Amulet, Quebec, Canada. *Appl. Geochem.* **5,** 27–346.

Boursiquot S., Mullet M., Abdelmoula M., Génin J.-M., and Ehrhardt J.-J. (2001) The dry oxidation of tetragonal FeS_{1-x} mackinawite. *Phys. Chem. Miner.* **28,** 600–611.

Brienne S. H. R., Zhang Q., Butler I. S., Xu Z., and Finch J. A. (1994) X-ray photoelectron and infrared spectroscopic investigation of sphalerite activation with iron. *Langmuir* **10,** 3582–3586.

Buckley A. N. and Woods R. (1985a) X-ray photoelectron spectroscopy of oxidized pyrrhotite surfaces. I. Exposure to air. *Appl. Surf. Sci.* **22**(23), 280–287.

Buckley A. N. and Woods R. (1985b) X-ray photoelectron spectroscopy of oxidized pyrrhotite surfaces. II. Exposure to aqueous solutions. *Appl. Surf. Sci.* **20,** 472–480.

Burns R. G. and Fisher D. S. (1990) Iron-sulfur mineralogy of Mars: Magmatic evolution and chemical weathering products. *J. Geophys. Res.* **95,** 14415–14421.

Cahill C. L., Benning L. G., Barnes H. L., and Parise J. B. (2000) In situ time-resolved X-ray diffraction of iron sulfides during hydrothermal pyrite growth. *Chem. Geol.* **167,** 53–63.

Degenhardt J. and McQuillan A. J. (1999) In situ ATR-FTIR spectroscopic study of adsorption of perchlorate, sulfate, and thiosulfate ions onto chromium(III) oxide hydroxide thin films. *Langmuir* **15,** 4595–4602.

Eggleston C. M., Ehrhardt J.-J., and Stumm W. (1996) Surface structural controls on pyrite oxidation kinetics: An XPS-UPS, STM, and modeling study. *Am. Mineral.* **81,** 1036–1057.

Eggleston C. M., Hug S., Stumm W., Sulzberger B., and Dos Santos Afonso M. (1998) Surface complexation of sulfate by hematite surfaces: FTIR and STM observations. *Geochim. Cosmochim. Acta* **62,** 585–593.

El Jaroudi O., Picquenard E., Demoirtier A., Lelieur J.-P., and Corset J. (1999) Polysulfide anions. 1. Structure and vibrational spectra of the S_2^{2-} and S_3^{2-} anions. Influence of the cations on bond length and angle. *Inorg. Chem.* **38,** 2394–2401.

Galakhov V. R. and Kurmaev E. Z. (1987) X-ray L spectra of 3d-metal oxides and analysis of the surface oxidation of the alloys. *Poverhnost. Fiz. Khim. Mekhan.* **10,** 107–112.

Janzen M. P., Nicholson R. V., and Scharer J. M. (2000) Pyrrhotite reaction kinetics: Reaction rates for oxidation by oxygen, ferric iron, and for nonoxidative dissolution. *Geochim. Cosmochim. Acta* **64,** 1511–1522.

Jones C. F., LeCount S., Smart R. St. C., and White T. J. (1992) Compositional and structural alteration of pyrrhotite surfaces in solution: XPS and XRD studies. *Appl. Surf. Sci.* **55,** 65–85.

Kastner M., Adler D., and Fritzsche H. (1976) Valence-alteration model for localised gap states in lone-pair semiconductors. *Phys. Rev. Lett.* **37,** 1504–1507.

Kelsall G. H., Yin Q., Vaughan D. J., England K. E. R., and Brandon N. P. (1999) Electrochemical oxidation of pyrite (FeS_2) in aqueous electrolytes. *J. Electroanal. Chem.* **471,** 116–125.

Pashkov G. L., Kargin V. F., and Asanov I. P. (2001) Conditions for the formation of a nonequilibrium nonstoichiometric layer on pyrrhotite in acid solutions. *Russ. J. Electrochem.* **37,** 1269–1276.

Laputina I. P. (1991) *Microprobe Analysis in Mineralogy*. Nauka, Moscow, Russia.

Lowson R. T. (1982) Aqueous oxidation of pyrite by molecular oxygen. *Chem. Rev.* **82,** 461–497.

Luther G. W. III. (1987) Pyrite oxidation and reduction: Molecular orbital theory considerations. *Geochim. Cosmochim. Acta* **51,** 3193–3199.

Matsuo M., Kawakami M., and Sugimori K. (2000) Mossbauer spectroscopic study on chemical changes of iron compounds with the aid of sulfate-reducing bacteria. *Hyperfine Interactions.* **126,** 53–58.

Mikhlin Yu. (2000) Reactivity of pyrrhotite surfaces: An electrochemical study. *Phys. Chem. Chem. Phys.* **2,** 5672–5677.

Mikhlin Yu. L., Tomashevich Ye. V., Varnek V. A., and Asanov I. P. (1995) Alteration of hexagonal pyrrhotite under acidic etching. *Russ. J. Inorg. Chem.* **40,** 1247–1253.

Mikhlin Yu. L., Tomashevich Ye. V., Pashkov G. L., Okotrub A. V., Asanov I. P., and Mazalov L. N. (1998) Electronic structure of the non-equilibrium iron-deficient layer of hexagonal pyrrhotite. *Appl. Surf. Sci.* **125,** 73–84.

Mikhlin Yu., Varnek V., Asanov I., Tomashevich Ye., Okotrub A., Livshits A., Selyutin G., and Pashkov G. (2000) Reactivity of pyrrhotite (Fe_9S_{10}) surfaces: Spectroscopic studies. *Phys. Chem. Chem. Phys.* **2,** 4393–4398.

Mikhlin Yu. L., Kuklinskiy A. V., Pashkov G. L. and Asanov I. P. (2001) Pyrrhotite electrooxidation in acid solutions. *Russ. J. Electrochem.* **37,** 1277–1282.

Mishra K. K. and Osseo-Asare K. (1988) Aspects of the interfacial electrochemistry of semiconductor pyrite (FeS_2) surfaces. *J. Electrochem. Soc.* **135,** 2502–2509.

Mott N. F. and Davis E. A. (1979) *Electron Processes in Non-Crystalline Materials*. Clarendon Press, Oxford, UK.

Murad E. and Bishop J. L. (2000) The infrared spectrum of synthetic akaganéite, β-FeOOH. *Am. Mineral.* **85,** 716–721.

Murad E., Schwertmann U., Bigham J. M., and Carlson L. (1994) Mineralogical characteristics of poorly crystallized precipitates formed by oxidation of Fe^{2+} in acid sulfate waters. In *Environmental Geochemistry of Sulfide Oxidation* (eds. C. N. Alpers and D. W. Blowes), pp. 191–200. American Chemical Society, Washington, DC.

Mycroft J. R., Bancroft G. M., McIntyre N. S., Lorimer J. W., and Hill I. R. (1990) Detection of sulfur and polysulfides on electrochemically oxidized pyrite surfaces by X-ray photoelectron spectroscopy and Raman spectroscopy. *J. Electroanal. Chem.* **292,** 139–152.

Mycroft J. R., Nesbitt H. W., and Pratt A. R. (1995) X-ray photoelectron and Auger electron spectroscopy of air-oxidized pyrrhotite: Distribution of oxidized species with depth. *Geochim. Cosmochim. Acta* **59,** 721–733.

Nakamoto K. (1986) *Infrared and Raman Spectra of Inorganic and Coordination Compounds*. Wiley, New York.

Nicholson R. V. and Scharer J. M. (1994) Laboratory studies of pyrrhotite oxidation kinetics. In *Environmental Geochemistry of Sulfide Oxidation* (eds. C. N. Alpers and D. W. Blowes), pp. 14–30. American Chemical Society, Washington, DC.

Nicol M. J. and Scott P. D. (1979) The kinetics and mechanisms of the non-oxidative dissolution of some iron sulphides in aqueous acidic solutions. *J. S. Afr. Inst. Min. Met.* **79,** 298–305.

Nowok J. and Stenberg V. I. (1988) Fe(III) ESR-signal splitting in unoxidized and oxidized semimagnetic pyrrhotite, Fe_7S_8. *Solid State Commun.* **66,** 835–840.

Persson P. and Lövgren L. (1996) Potentiometric and spectroscopic studies of sulfate complexation at the goethite-water interface. *Geochim. Cosmochim. Acta* **60,** 2789–2799.

Pratt A. R. and Nesbitt H. W. (1997) Pyrrhotite leaching in acid mixtures of HCl and H_2SO_4. *Am. J. Sci.* **297,** 807–820.

Pratt A. R., Muir I. J., and Nesbitt H. W. (1994a) X-ray photoelectron and Auger electron studies of pyrrhotite and mechanism of air oxidation. *Geochim. Cosmochim. Acta* **58,** 827–841.

Pratt A. R., Nesbitt H. W., and Muir I. J. (1994b) Generation of acids from mine waste: Oxidative leaching of pyrrhotite in dilute H_2SO_4 solutions (pH 3). *Geochim. Cosmochim. Acta* **58,** 5147–5159.

Schaufuss A. G., Nesbitt H. W., Kartio I., Laajalehto K., Bancroft G. M., and Szargan R. (1998a) Incipient oxidation of fractured pyrite surfaces in air. *J. Electron Spectr. Rel. Phen.* **96,** 69–82.

Schaufuss A. G., Nesbitt H. W., Kartio I., Laajalehto K., Bancroft G. M., and Szargan R. (1998b) Reactivity of surface chemical states on fractured pyrite. *Surf. Sci.* **411,** 321–325.

Shao-Horn Y. and Horn Q. C. (2001) Chemical, structural and electrochemical comparison of natural and synthetic FeS_2 pyrite in lithium cells. *Electrochim. Acta* **46,** 2613–2621.

Soezima H., Araki T., and Masaki T. (1978) Profile characteristic parameter and read out accuracy in electron microprobe state analysis by soft X-rays. *Jpn. J. Appl. Phys.* **17**(Suppl. 2), 408–411.

Schoonen M. A. A. and Barnes H. L. (1991a) Reactions forming pyrite and marcasite from solution: I. Nucleation of FeS_2 below 100°C. *Geochim. Cosmochim. Acta* **55,** 1495–1504.

Schoonen M. A. A. and Barnes H. L. (1991b) Reactions forming pyrite and marcasite from solution: II. Via FeS precursors below 100°C. *Geochim. Cosmochim. Acta* **55,** 1505–1514.

Steager H. F. (1982) Oxidation of sulfide minerals VII. Effect of temperature and relative humidity on the oxidation of pyrrhotite. *Chem. Geol.* **35,** 281–295.

Steager H. F. and Desjardins L. E. (1978) Oxidation of sulfide minerals, 4. Pyrite, chalcopyrite and pyrrhotite. *Chem. Geol.* **23,** 225–237.

Tejedor-Tejedor M. I. and Anderson M. A. (1986) "In situ" attenuated total reflection Fourier transform infrared studies of the goethite (α-FeOOH)-aqueous solution interface. *Langmuir* **2,** 203–210.

Thomas B., Ellmer K., Bohne W., Röhrich J., Kunst M., and Tributsch H. (1999) Photoeffects in cobalt doped pyrite (FeS_2) films. *Solid State Commun.* **111,** 235–240.

Thomas J. E., Jones C. F., Skinner W. M., and Smart R. St. C. (1998) The role of surface sulfur species in the inhibition of pyrrhotite dissolution in acid conditions. *Geochim. Cosmochim. Acta* **62,** 1555–1565.

Thomas J. E., Skinner W. M., and Smart R. St. C. (2001) A mechanism to explain sudden changes in rates and products for pyrrhotite dissolution in acid solution. *Geochim. Cosmochim. Acta* **65,** 1–12.

Thornber M. R. and Wildman J. E. (1979) Supergene alteration of sulfides, 4. Laboratory study of the weathering of nickel ores. *Chem. Geol.* **24,** 97–110.

Timoshenko E. M., Sobol S. I., Nagornaya T. V., and Morozova V. A. (1991) An investigation of solid products of sulfur dioxide pressure leaching of pyrrhotite. *Sov. Non-Ferr. Met.* **11,** 17–20.

Toniazzo V., Mustin C., Portal J. M., Humbert B., Benoit R., and Erre R. (1999) Elemental sulfur at the pyrite surfaces: Speciation and quantification. *Appl. Surf. Sci.* **143,** 229–237.

Tsendin K. D., et al (1996) *Electron Phenomena in Chalcogenide Glassy Semiconductors*. Nauka, St. Petersburg, Russia.

Vaughan D. J. and Craig J. R. (1978) *Mineral Chemistry of Metal Sulfides*. Cambridge University Press, Cambridge, UK.

Widler A. M. and Seward T. M. (2002) The adsorption of gold(I) hydrosulphide complexes by iron sulphide surfaces. *Geochim. Cosmochim. Acta* **66,** 383–402.

Wilkin R. T. and Barnes H. L. (1996) Pyrite formation by reactions of iron monosulfides with dissolved inorganic and organic sulfur species. *Geochim. Cosmochim. Acta* **60,** 4167–4179.

Woods R. (1988) Flotation of sulfide minerals. In *Reagents in Mineral Technology* (eds. P. Somasundaran and B. M. Moudgil), pp. 39–78. Dekker, New York.